Computer Physics Communications 200 (2016) 108–116

Contents lists available at ScienceDirect

Computer Physics Communications

journal homepage: www.elsevier.com/locate/cpc

A compact fourth-order finite difference scheme for the three-dimensional Cahn–Hilliard equation

Yibao Li [a], Hyun Geun Lee [b], Binhu Xia [a], Junseok Kim [c,*]

[a] School of Mathematics and Statistics, Xi'an Jiaotong University, Xi'an 710049, China
[b] Institute of Mathematical Sciences, Ewha Womans University, Seoul 120-750, Republic of Korea
[c] Department of Mathematics, Korea University, Seoul 136-713, Republic of Korea

HIGHLIGHTS

- We present a three-dimensional compact scheme for the Cahn–Hilliard equation.
- The scheme has second-order accuracy in time and fourth-order accuracy in space.
- We implement the compact scheme in an adaptive mesh refinement framework.

ARTICLE INFO

Article history:
Received 19 July 2015
Accepted 14 November 2015
Available online 23 November 2015

Keywords:
Cahn–Hilliard equation
Finite difference method
Fourth-order compact scheme
Multigrid
Adaptive mesh refinement

ABSTRACT

This work extends the previous two-dimensional compact scheme for the Cahn–Hilliard equation (Lee et al., 2014) to three-dimensional space. The proposed scheme, derived by combining a compact formula and a linearly stabilized splitting scheme, has second-order accuracy in time and fourth-order accuracy in space. The discrete system is conservative and practically stable. We also implement the compact scheme in a three-dimensional adaptive mesh refinement framework. The resulting system of discrete equations is solved by using a multigrid. We demonstrate the performance of our proposed algorithm by several numerical experiments.

1. Introduction

In this paper, our goal is to develop a high-order accurate compact scheme, i.e., second-order accurate in time and fourth-order accurate in space, for the three-dimensional Cahn–Hilliard (CH) equation [1,2]:

$$\frac{\partial \phi}{\partial t}(\mathbf{x},t) = M\Delta\mu(\mathbf{x},t), \quad \mathbf{x}\in\Omega,\ 0<t\le T, \tag{1}$$

$$\mu(\mathbf{x},t) = F'(\phi(\mathbf{x},t)) - \epsilon^2\Delta\phi(\mathbf{x},t), \tag{2}$$

where the order parameter $\phi(\mathbf{x},t)$ is the difference of two concentrations in a binary mixture in a domain $\Omega\subset\mathbb{R}^3$. Further, M is the mobility, μ is the chemical potential, $F(\phi)=0.25(\phi^2-1)^2$ is the free energy density, and ϵ is a positive constant related to the interfacial thickness. For the sake of convenience, we let $M=1$. To simplify the presentation, here we consider the periodic boundary condition for both the order parameter and the chemical potential. The CH equation was introduced to model phase separation phenomena in binary alloys [1,2] and it can be derived from the constrained gradient flow in the $\bar{H}^{-1}$ Hilbert space of the Helmholtz free energy functional:

$$\mathcal{E}(\phi) = \int_\Omega \left(F(\phi) + \frac{\epsilon^2}{2}|\nabla\phi|^2\right) d\mathbf{x}.$$

The properties of the solution $\phi(\mathbf{x},t)$ of the CH Eqs. (1) and (2) are such that the total mass $\int_\Omega \phi\, d\mathbf{x}$ is conserved

$$\frac{d}{dt}\int_\Omega \phi\, d\mathbf{x} = \int_\Omega \phi_t\, d\mathbf{x} = M\int_\Omega \Delta\mu\, d\mathbf{x} = M\int_{\partial\Omega}\frac{\partial\mu}{\partial\mathbf{n}}\, ds = 0$$

and the total energy $\mathcal{E}(t)$ decreases with time

$$\begin{aligned}\frac{d}{dt}\mathcal{E}(\phi) &= \int_\Omega (F'(\phi)\phi_t + \epsilon^2\nabla\phi\cdot\nabla\phi_t)d\mathbf{x}\\ &= \int_\Omega \mu\phi_t d\mathbf{x} + \int_{\partial\Omega}\epsilon^2\frac{\partial\phi}{\partial\mathbf{n}}\phi_t ds = \int_\Omega \mu M\Delta\mu d\mathbf{x}\end{aligned}$$

* Corresponding author. Tel.: +82 2 3290 3077; fax: +82 2 929 8562.
E-mail addresses: yibaoli@mail.xjtu.edu.cn (Y. Li), cfdkim@korea.ac.kr (J. Kim).
URLs: http://gr.xjtu.edu.cn/web/yibaoli (Y. Li), http://math.korea.ac.kr/~cfdkim (J. Kim).

http://dx.doi.org/10.1016/j.cpc.2015.11.006
0010-4655/

$$= \int_{\partial\Omega} \mu M \frac{\partial \mu}{\partial \mathbf{n}} ds - \int_{\Omega} M \nabla\mu \cdot \nabla\mu d\mathbf{x}$$
$$= -\int_{\Omega} M|\nabla\mu|^2 d\mathbf{x} \le 0.$$

Here, $\mathbf{n}$ is the outward normal vector at the boundary. The CH equation has been widely used in many fields such as in the physical and materials sciences [3–5], fluid dynamics [6–9], biological simulations [10,11], image processing [12,13] and surface/volume reconstruction [14]. Therefore, it is very important to develop accurate and efficient numerical schemes to solve the CH equation.

Many research papers have been published on the numerical methods for the CH equation [15–24]. Regarding time discretization, most of the schemes referenced above have used explicit, implicit–explicit, Crank–Nicolson or Adams–Bashforth methods. However, as the CH equation has fourth-order spatial derivatives and a nonlinear term, the use of an explicit time scheme leads to severe time step restrictions to ensure stability. Although the fully implicit approach can use a large time step, it only has first-order accuracy in time and therefore requires small time steps to guarantee accuracy. On the other hand, for higher-order numerical solutions, the Crank–Nicolson and Adams–Bashforth methods would be better choices.

Regarding space discretization, most of these numerical solutions have second-order accuracy in spatial discretizations. Compact difference methods have been developed for biharmonic [25,26], convection–diffusion [27,28], Poisson [29–31], Navier–Stokes [32], and Helmholtz [33] equations. These methods achieve high-order accuracy without a significant increase in the number of grid points in each coordinate direction. It should be pointed out that in the finite difference framework, we can straightforwardly derive high-order schemes by increasing the number of grid points in each coordinate direction. However, this may be problematic when those points are close to the domain boundary. Possible ways in which to overcome this challenge would either be to switch to a different solver in proximity of the boundary or to introduce a second boundary layer by interpolation [31]. This, however, generally lowers the overall accuracy of the solution. Furthermore, when multigrid or adaptive mesh refinement (AMR) methods are used, this problem becomes more obvious, because the same spatial operators would have to be performed on both coarse and fine grid levels, which is much more difficult. Therefore, compact high-order schemes, which need less information from neighboring grid points, are better choices.

To date, there are few studies of the CH equation, which have used the high-order difference method. Li et al. [34] established a three-level linearized compact difference scheme for the CH equation. Song [35] discretized the CH equation by using a fourth-order compact difference scheme in space and first-order, second-order, or third-order implicit–explicit Runge–Kutta schemes in time. Lee et al. [36] presented a fourth-order spatially accurate and practically stable compact difference scheme for the CH equation in two-dimensional space. However, we are not aware of any results for the three-dimensional CH equation on second-order time and fourth-order space discretization, a combination known to exhibit excellent stability.

The objective of this paper is to propose a high-order compact scheme for the CH equation in three-dimensional space. We demonstrate that our scheme has second-order accuracy in time and fourth-order accuracy in space, which is an extension of the previous results for two-dimensional space [36]. The discrete system has the ability to preserve mass conservation, uses large-size time steps and exhibits excellent stability. We solve the resulting system of discrete equations by a linear multigrid. In addition, we implement our approach in the AMR framework. We demonstrate the performance of our proposed algorithm by conducting several numerical experiments.

This paper is organized as follows. In Section 2, we derive the fourth-order compact finite difference scheme and its properties are proved. In Section 3, we present the numerical experiments. Finally, conclusions are drawn in Section 4.

2. Numerical solution

2.1. Compact finite difference scheme

We discretize the CH equation in three-dimensional domain $\Omega = (0, L_x) \times (0, L_y) \times (0, L_z)$. Let N_x, N_y, and N_z be positive even integers, $h = L_x/N_x = L_y/N_y = L_z/N_z$ be the uniform mesh size. We denote a discrete computational domain by $\Omega_h = \{(x_i, y_j, z_k) : x_i = (i-0.5)h,\ y_j = (j-0.5)h,\ z_k = (k-0.5)h,\ 1 \le i \le N_x,\ 1 \le j \le N_y\ 1 \le k \le N_z\}$, which is the set of cell-centers. Let ϕ^n_{ijk} be the approximation of $\phi(x_i, y_j, z_k, n\Delta t)$, where $\Delta t = T/N_t$ is the time step, T is the final time, and N_t is the total number of time steps.

We use the 27-point discrete Laplacian operator in three-dimensional space [37], i.e.,

$$\begin{aligned}\Delta_c\phi_{ijk} = [&14(\phi_{i+1,jk} + \phi_{i-1,jk} + \phi_{i,j+1,k} + \phi_{i,j-1,k} \\ &+ \phi_{ij,k+1} + \phi_{ij,k-1}) + 3(\phi_{i+1,j+1,k} + \phi_{i+1,j-1,k} + \phi_{i+1,j,k+1} \\ &+ \phi_{i+1,j,k-1} + \phi_{i-1,j+1,k} + \phi_{i-1,j-1,k} \\ &+ \phi_{i-1,j,k+1} + \phi_{i-1,j,k-1} + \phi_{i,j+1,k+1} + \phi_{i,j-1,k-1} \\ &+ \phi_{i,j+1,k-1} + \phi_{i,j-1,k+1}) + \phi_{i-1,j+1,k+1} + \phi_{i-1,j-1,k-1} \\ &+ \phi_{i-1,j+1,k-1} + \phi_{i-1,j-1,k+1} + \phi_{i+1,j+1,k+1} \\ &+ \phi_{i+1,j-1,k-1} + \phi_{i+1,j+1,k-1} + \phi_{i+1,j-1,k+1} - 128\phi_{ijk}]/(30h^2). \quad (3)\end{aligned}$$

The stencil numbering for the three-dimensional Laplacian operator is also labeled according to the diagram in Fig. 1. By the Taylor series in three variables, we can obtain

$$\begin{aligned}&\phi(x+h, y+h, z+h) \\ &= \sum_{m=0}^{5} \frac{1}{m!} \left(h\frac{\partial}{\partial x} + h\frac{\partial}{\partial y} + h\frac{\partial}{\partial z} \right)^m \phi(x, y, z) + O(h^6). \quad (4)\end{aligned}$$

Substituting (4) into (3), we obtain the high-order Laplace approximation at node ijk:

$$\begin{aligned}\Delta\phi_{ijk} &= \left(\frac{\partial^2\phi}{\partial x^2} + \frac{\partial^2\phi}{\partial y^2} + \frac{\partial^2\phi}{\partial z^2} \right)_{ijk} \\ &= \Delta_c\phi_{ijk} - \frac{h^2}{12}\Delta^2\phi_{ijk} + O(h^4). \quad (5)\end{aligned}$$

Here $\Delta^2\phi = \Delta(\Delta\phi)$ is the biharmonic operator. Now, we derive the fourth-order spatially accurate and practically stable compact finite difference scheme for the CH equation. At node ijk, we can discretize Eq. (1) as

$$\begin{aligned}(\phi_t)_{ijk} &= \Delta\mu_{ijk} = \Delta_c\mu_{ijk} - \frac{h^2}{12}\Delta^2\mu_{ijk} + O(h^4) \\ &= \Delta_c\mu_{ijk} - \frac{h^2}{12}(\Delta\phi_t)_{ijk} + O(h^4) \\ &= \Delta_c\mu_{ijk} - \frac{h^2}{12}(\Delta_c\phi_t)_{ijk} + O(h^4). \quad (6)\end{aligned}$$

Because Δ_c is the second-order approximation of the Laplacian operator, Eq. (6) is sufficient to guarantee fourth-order accuracy of the solution. Furthermore, the backward differentiation formula

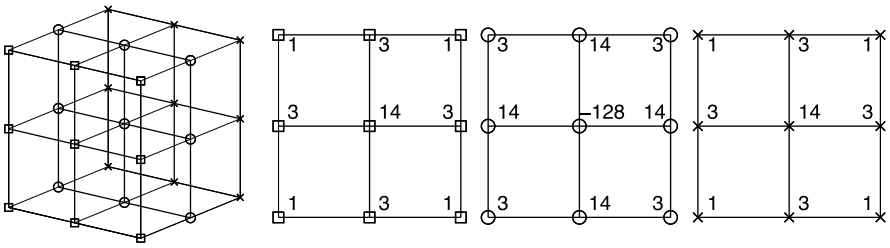

Fig. 1. Stencil numbering for the three-dimensional Laplacian operator.

offers a convenient choice to obtain second-order accuracy in time. Thus, the discretization of Eq. (6) is written as [38]:

$$\frac{1}{\Delta t}\left(\frac{3}{2}\phi_{ijk}^{n+1}-2\phi_{ijk}^{n}+\frac{1}{2}\phi_{ijk}^{n-1}\right) = \Delta_c\mu_{ijk}^{n+1}-\frac{h^2}{12\Delta t}\left(\frac{3}{2}\Delta_c\phi_{ijk}^{n+1}-2\Delta_c\phi_{ijk}^{n}+\frac{1}{2}\Delta_c\phi_{ijk}^{n-1}\right) + O(\Delta t^2+h^4), \tag{7}$$

where $\phi^{-1}=\phi^0$. To obtain a high-order stable scheme, we use a linearly stabilized splitting scheme of Eq. (2) [39]:

$$\mu^{n+1} = 2(F'(\phi^n)-2\phi^n)-(F'(\phi^{n-1})-2\phi^{n-1}) + 2\phi^{n+1}-\epsilon^2\Delta\phi^{n+1}. \tag{8}$$

Substituting Eq. (5) into Eq. (8), we obtain the fourth-order form for Eq. (8) at node *ijk*,

$$\begin{aligned}\mu_{ijk}^{n+1} &= 2(F'(\phi)-2\phi)_{ijk}^{n}-(F'(\phi)-2\phi)_{ijk}^{n-1}+2\phi_{ijk}^{n+1} \\ &\quad -\epsilon^2\Delta_c\phi_{ijk}^{n+1}+\frac{\epsilon^2h^2}{12}\Delta^2\phi_{ijk}^{n+1}+O(h^4) \\ &= 2(F'(\phi)-2\phi)_{ijk}^{n}-(F'(\phi)-2\phi)_{ijk}^{n-1} \\ &\quad +2\phi_{ijk}^{n+1}-\epsilon^2\Delta_c\phi_{ijk}^{n+1}+O(h^4) \\ &\quad +\frac{h^2}{12}\Delta_c\left(2(F'(\phi)-2\phi)_{ijk}^{n}-(F'(\phi)-2\phi)_{ijk}^{n-1}\right. \\ &\quad \left.+\ 2\phi_{ijk}^{n+1}-\mu_{ijk}^{n+1}\right).\end{aligned} \tag{9}$$

Finally, our proposed schemes are written as:

$$\frac{1}{\Delta t}\left(\frac{3}{2}\phi_{ijk}^{n+1}-2\phi_{ijk}^{n}+\frac{1}{2}\phi_{ijk}^{n-1}\right) = \Delta_c\mu_{ijk}^{n+1}-\frac{h^2}{12\Delta t}\left(\frac{3}{2}\Delta_c\phi_{ijk}^{n+1}-2\Delta_c\phi_{ijk}^{n}+\frac{1}{2}\Delta_c\phi_{ijk}^{n-1}\right), \tag{10}$$

$$\begin{aligned}\mu_{ijk}^{n+1} &= 2(F'(\phi)-2\phi)_{ijk}^{n}-(F'(\phi)-2\phi)_{ijk}^{n-1} \\ &\quad +2\phi_{ijk}^{n+1}-\epsilon^2\Delta_c\phi_{ijk}^{n+1}+\frac{h^2}{12}\Delta_c\left(2(F'(\phi)\right. \\ &\quad \left.-\ 2\phi)_{ijk}^{n}-(F'(\phi)-2\phi)_{ijk}^{n-1}+2\phi_{ijk}^{n+1}-\mu_{ijk}^{n+1}\right).\end{aligned} \tag{11}$$

Here, we consider the periodic boundary conditions to simplify the presentation. We use an approximation storage multigrid method to solve the linear discrete system (10) and (11) at the implicit time level. For additional details and background information pertaining to the multigrid method, please refer to the reference text [40]. We define the discrete total energy functional by

$$\mathcal{E}^h(\phi^n)=(F(\phi^n),\mathbf{1})_h+\frac{\epsilon^2}{2}(\nabla_c\phi^n,\nabla_c\phi^n)_e.$$

Here $\mathbf{1}$ is a vector with all entries equal to 1 and the notation $(\phi,\psi)_h$ is the discrete l_2-inner products, which is defined as

$$(\phi,\psi)_h := h^3\sum_{i=1}^{N_x}\sum_{j=1}^{N_y}\sum_{k=1}^{N_z}\phi_{ijk}\psi_{ijk}. \tag{12}$$

The inner product for $\nabla_c\phi$ on the staggered grid is defined by

$$(\nabla_c\phi,\nabla_c\psi)_e = h^3\sum_{i=1}^{N_x}\sum_{j=1}^{N_y}\sum_{k=1}^{N_z}\left(D_x\phi_{i+\frac{1}{2},jk}D_x\psi_{i+\frac{1}{2},jk} + D_y\phi_{i,j+\frac{1}{2},k}D_y\psi_{i,j+\frac{1}{2},k}+D_z\phi_{ij,k+\frac{1}{2}}D_z\psi_{ij,k+\frac{1}{2}}\right), \tag{13}$$

where the discrete differentiation operators $D_x\phi_{i+\frac{1}{2},jk}$, $D_y\phi_{i,j+\frac{1}{2},k}$, and $D_z\phi_{i,j,k+\frac{1}{2}}$ are defined as

$$\begin{aligned}D_x\phi_{i+\frac{1}{2},jk} &= [128(\phi_{i+1,jk}-\phi_{ijk})+11(\phi_{i+1,j+1,k}-\phi_{i,j+1,k} \\ &\quad +\phi_{i+1,j-1,k}-\phi_{i,j-1,k} \\ &\quad +\phi_{i+1,j,k+1}-\phi_{i,j,k+1}+\phi_{i+1,j,k-1}-\phi_{ij,k-1}) \\ &\quad +2(\phi_{i+1,j+1,k+1}-\phi_{i,j+1,k+1} \\ &\quad +\phi_{i+1,j-1,k+1}-\phi_{i,j-1,k+1} \\ &\quad +\phi_{i+1,j+1,k-1}-\phi_{i,j+1,k-1} \\ &\quad +\phi_{i+1,j-1,k-1}-\phi_{i,j-1,k-1})]/(180h), \\ D_y\phi_{i,j+\frac{1}{2},k} &= [128(\phi_{i,j+1,k}-\phi_{ijk})+11(\phi_{i+1,j+1,k}-\phi_{i+1,j,k} \\ &\quad +\phi_{i-1,j+1,k}-\phi_{i-1,j,k} \\ &\quad +\phi_{i,j+1,k+1}-\phi_{i,j,k+1}+\phi_{i,j+1,k-1}-\phi_{ij,k-1}) \\ &\quad +2(\phi_{i+1,j+1,k+1}-\phi_{i+1,j,k+1} \\ &\quad +\phi_{i-1,j+1,k+1}-\phi_{i-1,j,k+1} \\ &\quad +\phi_{i+1,j+1,k-1}-\phi_{i+1,j,k-1} \\ &\quad +\phi_{i-1,j+1,k-1}-\phi_{i-1,j,k-1})]/(180h),\end{aligned}$$

and

$$\begin{aligned}D_z\phi_{i,j,k+\frac{1}{2}} &= [128(\phi_{i,j,k+1}-\phi_{ijk})+11(\phi_{i,j+1,k+1}-\phi_{i,j+1,k} \\ &\quad +\phi_{i,j-1,k+1}-\phi_{i,j-1,k} \\ &\quad +\phi_{i+1,j,k+1}-\phi_{i+1,j,k}+\phi_{i-1,j,k+1}-\phi_{i-1,j,k}) \\ &\quad +2(\phi_{i+1,j+1,k+1}-\phi_{i+1,j+1,k} \\ &\quad +\phi_{i+1,j-1,k+1}-\phi_{i+1,j-1,k} \\ &\quad +\phi_{i-1,j+1,k+1}-\phi_{i-1,j+1,k} \\ &\quad +\phi_{i-1,j-1,k+1}-\phi_{i-1,j-1,k})]/(180h).\end{aligned}$$

Using these definitions, we can rewrite the discrete Laplacian $\Delta_c\phi_{ijk}$ as

$$\Delta_c\phi_{ijk} = \frac{D_x\phi_{i+\frac{1}{2},j,k}-D_x\phi_{i-\frac{1}{2},j,k}}{h}+\frac{D_y\phi_{i,j+\frac{1}{2},k}-D_y\phi_{i,j-\frac{1}{2},k}}{h} + \frac{D_z\phi_{i,j,k+\frac{1}{2}}-D_z\phi_{i,j,k-\frac{1}{2}}}{h}.$$

2.2. Mass conservation

The ability to conserve the total mass is an important property of the CH equation. Here, we will prove that our proposed method satisfies the mass conservation, i.e., $(\phi^{n+1},\mathbf{1})_h = (\phi^n,\mathbf{1})_h$. By combining Eq. (10) and the discrete version of the integration by

parts, we are able to obtain

$$\left(\frac{3}{2}\phi^{n+1}-2\phi^{n}+\frac{1}{2}\phi^{n-1},\mathbf{1}\right)_h=\Delta t(\Delta_c\mu^{n+1},\mathbf{1})_h$$
$$-\frac{h^2}{12}\left(\frac{3}{2}\Delta_c\phi^{n+1}-2\Delta_c\phi^{n}+\frac{1}{2}\Delta_c\phi^{n-1},\mathbf{1}\right)_h. \quad (14)$$

For $(\Delta_c\mu^{n+1},\mathbf{1})_h$, we can obtain that

$$\begin{aligned}(\Delta_c\mu^{n+1},\mathbf{1})_h &= h^3\sum_{i=1}^{N_x}\sum_{j=1}^{N_y}\sum_{k=1}^{N_z}\Delta_c\mu^{n+1}_{ijk}\\ &= h^2\sum_{i=1}^{N_x}\sum_{j=1}^{N_y}\sum_{k=1}^{N_z}\Big(D_x\mu^{n+1}_{i+\frac{1}{2},j,k}-D_x\mu^{n+1}_{i-\frac{1}{2},j,k}+D_y\mu^{n+1}_{i,j+\frac{1}{2},k}\\ &\quad -D_y\mu^{n+1}_{i,j-\frac{1}{2},k}+D_z\mu^{n+1}_{i,j,k+\frac{1}{2}}-D_z\mu^{n}_{i,j,k-\frac{1}{2}}\Big)\\ &= h^2\sum_{j=1}^{N_y}\sum_{k=1}^{N_z}\left(D_x\mu^{n+1}_{N_x+\frac{1}{2},j,k}-D_x\mu^{n+1}_{\frac{1}{2},j,k}\right)\\ &\quad +h^2\sum_{i=1}^{N_x}\sum_{k=1}^{N_z}\left(D_y\mu^{n+1}_{i,N_y+\frac{1}{2},k}-D_y\mu^{n+1}_{i,\frac{1}{2},k}\right)\\ &\quad +h^2\sum_{i=1}^{N_x}\sum_{j=1}^{N_y}\left(D_z\mu^{n+1}_{ij,N_z+\frac{1}{2}}-D_z\mu^{n+1}_{ij,\frac{1}{2}}\right)=0,\end{aligned}$$

where we have used the periodic boundary conditions for the chemical potential and telescoping cancellation. Using proofs similar to those above and summing by parts for Eq. (14), we obtain $(3\phi^{n+1},\mathbf{1})_h=(4\phi^{n},\mathbf{1})_h-(\phi^{n-1},\mathbf{1})_h$. Then we have $(\phi^{n+1},\mathbf{1})_h=(\phi^{n},\mathbf{1})_h$, if $(\phi^{n},\mathbf{1})_h=(\phi^{n-1},\mathbf{1})_h$. Since $(\phi^{0},\mathbf{1})_h=(\phi^{-1},\mathbf{1})_h$, we have the chain of equalities $(\phi^{n+1},\mathbf{1})_h=(\phi^{n},\mathbf{1})_h=\cdots=(\phi^{0},\mathbf{1})_h$. Thus, our proposed method satisfies the conservation of total mass.

3. Numerical results

This section presents details of the following numerical experiments: non-increasing of discrete energy and mass conservation, a convergence test, a test of the stability of the proposed scheme, spinodal decompositions, an extension to the adaptive mesh refinement method, an application for triply-periodic minimal surfaces, and an application for volume reconstruction from slice data. Unless otherwise specified, we consider $\epsilon=\epsilon_m=hm/[2\sqrt{2}\tanh^{-1}(0.9)]$ to ensure that the number of grid points across the interfacial regions is approximately m.

3.1. Non-increasing of discrete energy and mass conservation

We start with a numerical simulation to show the non-increasing of discrete energy and mass conservation of our proposed method. The initial condition is set as $\phi(x,y,z,0)=0.1+0.5\text{rand}(x,y,z)$ on the unit domain, where $\text{rand}(x,y,z)$ is a random number between -1 and 1. The calculation is run up to $t=0.9847$ with the time step $\Delta t=0.1h$ and mesh size $h=1/128$. Here ϵ_8 is used. The results shown in Fig. 2 suggest the phases are gathered together and the surface becomes smooth due to the CH equation. In Fig. 2, we also observe that with our proposed scheme, the total discrete energy is non-increasing and the mass concentration of the numerical solution remains.

3.2. Convergence test

Here we consider the spatial and temporal convergence tests of the proposed method. We obtained the spatial convergence rate by performing a number of simulations with increasingly finer grids $h=1/2^{n-1}$ for $n=5$, 6, 7, and 8 on a unit domain. The initial condition is $\phi(x,y,z,0)=\cos(2x\pi)\cos(2y\pi)\cos(2z\pi)$. For each grid we integrate over time $t=1.953\text{E}{-5}$ with time step $\Delta t=0.01h^2$ and $\epsilon=0.02$. Because there is no closed-form analytical solution for this problem, we define the error of the numerical solution on a grid as the discrete l_2-norm of the difference between the numerical solution u_h and the next finer grid cells covering it as follows: $e^{h/\frac{h}{2}}_{ijk}=\phi^{h}_{ijk}-(\phi^{h/2}_{2i,2j,2k}+\phi^{h/2}_{2i-1,2j,2k}+\phi^{h/2}_{2i,2j-1,2k}+\phi^{h/2}_{2i,2j,2k-1}+\phi^{h/2}_{2i-1,2j-1,2k}+\phi^{h/2}_{2i,2j-1,2k-1}+\phi^{h/2}_{2i-1,2j,2k-1}+\phi^{h/2}_{2i-1,2j-1,2k-1})/8$. The rate of convergence is defined as the ratio of successive errors: $\log_2(\|e^{h}\|_2/\|e^{\frac{h}{2}}\|_2)$. Here $\|e\|_2^2$ is a discrete l_2 norm and is defined as $\|e\|_2^2=\sum_{i=1}^{Nx}\sum_{j=1}^{Ny}\sum_{k=1}^{Nz}e^2_{ijk}/(NxNyNz)$. Because we refined the spatial and temporal grids by a factor of 4 and 2, respectively, the ratio of successive errors should increase by a factor of 4. The errors and rates of convergence obtained by these definitions are given in Table 1. The results suggest that the scheme has fourth-order accuracy in space and second-order accuracy in time, as expected from the discretization.

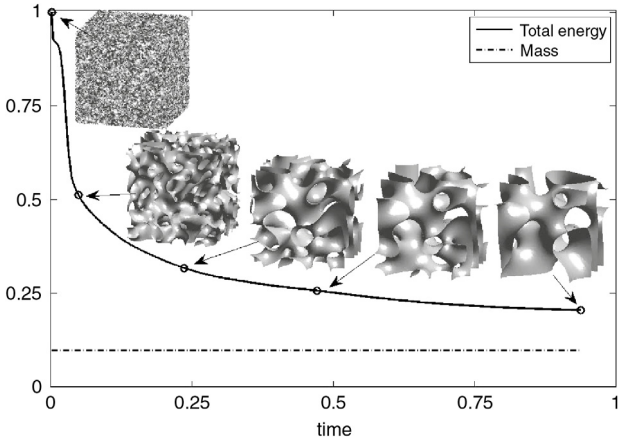

Fig. 2. Non-increasing of discrete energy and mass conservation of our proposed method. The inscribed small figures are the zero surfaces of the phase field at the indicated times. Note that we have normalized the total energy by using the total energy at the initial time.

Table 1
Error and convergence results with various mesh grids. $\Delta t=0.01h^2$ is fixed. Here 32^3–64^3 means $\|e^{h/\frac{h}{2}}\|_2$ with $h=1/32$.

Grid	32^3–64^3	64^3–128^3	128^3–256^3
l_2-error	4.763E−3	3.015E−4	1.974E−5
Rate	3.982	3.933	

3.3. Stability of the proposed scheme

We demonstrate the stability of our proposed scheme (10) and (11) by performing a numerical experiment using a set of different time steps $\Delta t=0.01h$, $0.1h$, h, and $10h$. The initial condition and parameters are set as in Section 3.1. The calculations are run up to time $t=7.812$ and the numerical solutions at time $t=1.562$ and 7.812 (from top to bottom) are shown in Fig. 3(a)–(d). Fig. 4 shows the total energy evolution, which suggests that our proposed scheme allows the use of large time steps. In addition, the evolving patterns are similar when $\Delta t=0.01h$ and $\Delta t=0.1h$ are used. Although a larger time step $\Delta t=10h$ can be used, the evolution is less accurate.

3.4. Efficiency of multigrid solver

The efficiency of the multigrid method was investigated by measuring the CPU time required to solve the following problem:

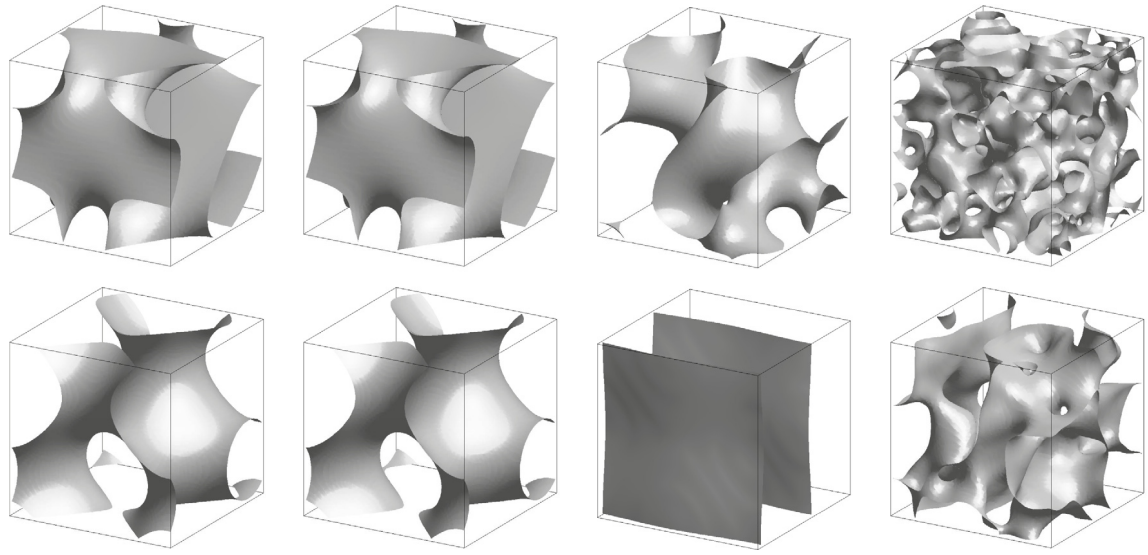

(a) $\Delta t = 0.01h$. (b) $\Delta t = 0.1h$. (c) $\Delta t = h$. (d) $\Delta t = 10h$.

Fig. 3. (a)–(d) Numerical solutions with different time steps at time $t = 1.562$ (top row) and 7.812 (bottom row).

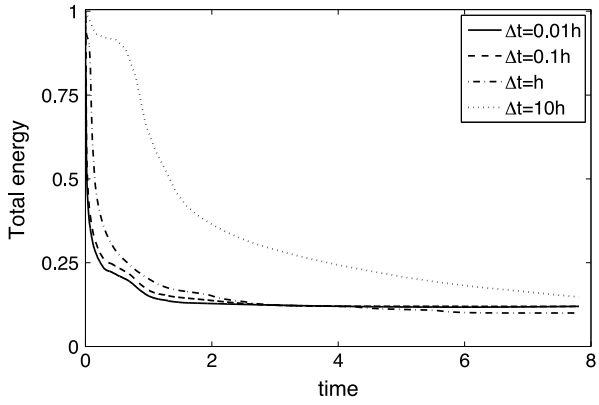

Fig. 4. Total energy evolution with different time steps $\Delta t = 0.01h$, $0.1h$, h, and $10h$. Here we have normalized the total energy by the total energy at $t = 0$.

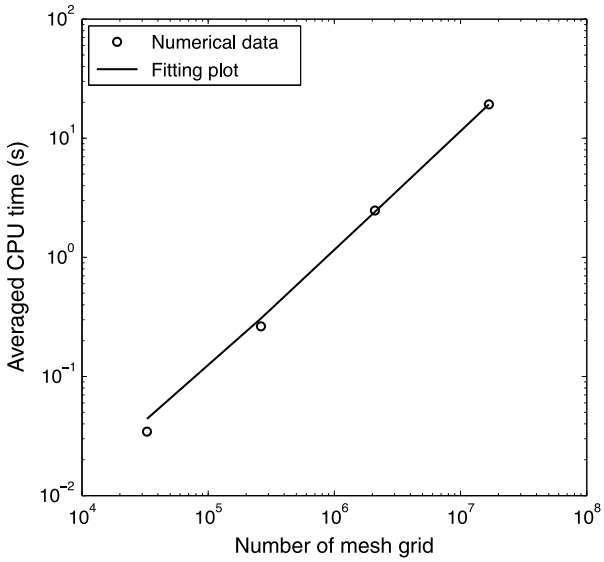

Fig. 5. Logarithm of averaged CPU time versus number of mesh grid points $(N_xN_yN_z)$ in multigrid solver.

$\phi(x, y, z, 0) = \cos(8x\pi)\cos(8y\pi)\cos(8z\pi)$ on the domain $(0, 2^{n-7}) \times (0, 2^{n-7}) \times (0, 2^{n-7})$ with $2^n \times 2^n \times 2^n$ meshes for $n = 5, 6, 7,$ and 8. With these definitions, $h = 1/128$ is fixed. And $\epsilon = 0.01$ and $\Delta t = 0.1h$ are chosen. We record the time by the CPU after ten time steps. Note that each iteration is run until the maximum error of the residual is less than 10^{-6}. Because we refined the spatial grids by a factor of eight, computational times should ideally also be increased by a factor of eight due to the discretizations (10) and (11) and the multigrid method that was used. Fig. 5 shows the averaged CPU times versus the number of points on the mesh grid $(N_xN_yN_z)$. The linearity of the plot implies that the multigrid solver achieves the $O(N_xN_yN_z)$ efficiency.

3.5. Spinodal decomposition

Next, we performed a numerical experiment using an example of spinodal decomposition of a binary mixture. Spinodal decomposition is a mechanism by which a solution of two or more components separates into different phases [1,2,41]. Here, we will consider this problem for the CH equation with the initial condition $\phi(x, y, z, 0) = \phi_{ave} + 0.5\text{rand}(x, y, z)$ on the unit domain. Then, the initial condition is a random perturbation from the average ϕ_{ave}. Simulations with $\phi_{ave} = -0.5$, 0, and 0.5 are run up to time $t = 156.25$. Here $h = 1/128$ and ϵ_8 are chosen. The depictions in Fig. 6(a)–(c) show the evolutions of spinodal decomposition with $\phi_{ave} = -0.5$, 0, and 0.5. Observing these results, we can see that the positive phases are separated and gathered together. Furthermore, an increase in the initial average ϕ_{ave} causes the volume of the positive phases to become larger, because of the conservation of mass. Fig. 6(a), for the case $\phi_{ave} = -0.5$, shows that the four equivalent positive phases remain, whereas Fig. 6(c), for the case $\phi_{ave} = 0.5$, presents the continuity of the positive phases. When ϕ_{ave} is zero, which means the positive and negative phases are equal, the positive phase converges to a bar shape.

3.6. Adaptive mesh refinement with high order

The AMR method [42,43] is more efficient than a method based on uniform mesh because it allows multi-resolution in interesting regions without requiring a fine grid resolution across the whole domain. This advantage has been widely exploited [44–46]. Our

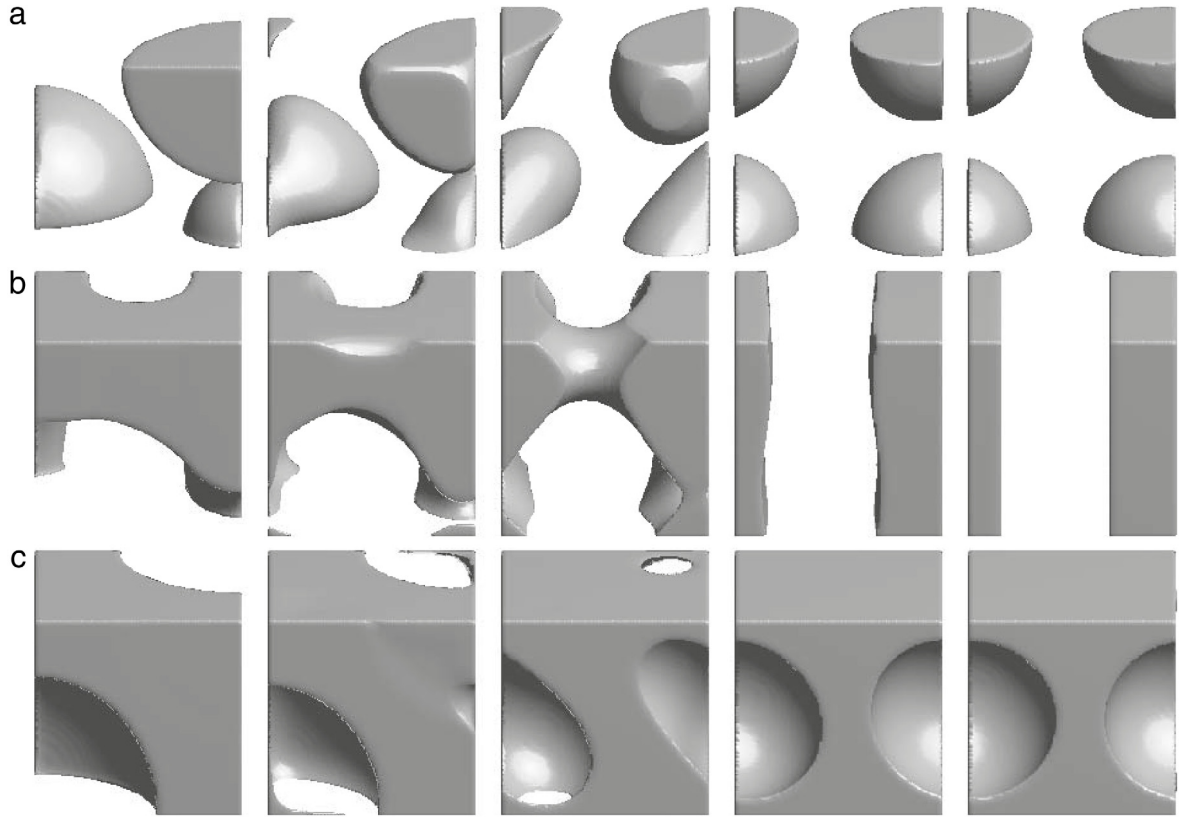

Fig. 6. Spinodal decomposition with different average ϕ_{ave}. (a) $\phi_{ave} = -0.5$. (b) $\phi_{ave} = 0$. (c) $\phi_{ave} = 0.5$. The gray domain corresponds to the positive phase. From left to right, the computational times are $t = 0.156,\ 1.563,\ 15.625,\ 46.875$, and 156.25, respectively.

method can be straightforwardly applied to an AMR framework. The initial condition is chosen as $\phi(x, y, z, 0) = 0.5\text{rand}(x, y, z)$. We performed the simulation on the unit domain with the base mesh grids $16 \times 16 \times 16$. There are four levels of refinement on the computational domain, with a respective mesh spacing of $1/16$, $1/32$, $1/64$, $1/128$, and $1/256$. The other parameters are taken as $\Delta t = 0.1/256$ and $\epsilon = 0.01$. Fig. 7 shows the evolution resulting from the use of the AMR method and the consequent dynamical adjustment of the hierarchical structure of the grid around the interface transition region. This simulation demonstrates that our proposed higher-order numerical scheme can be straightforwardly applied to AMR framework.

3.7. Triply-periodic minimal surfaces

One of the applications of the CH equation is to obtain triply-periodic minimal surfaces. The surfaces, which have a constant mean curvature everywhere on the surface and are periodic in three independent directions, are often referred to as triply periodic minimal surfaces. Triply-periodic minimal surfaces [47] are of special interest to physical scientists, materials scientists and mathematicians, because the geometry of triply periodic minimal surfaces strongly influences the physical properties of the material. Yang *et al.* [5] generated triply periodic constant mean curvature surfaces using a Cahn–Hilliard method. Starting from the periodic nodal surface approximation to minimal surfaces, they generated various constant mean curvature surfaces with given volume fractions. We generate initial configurations with the desired topology by taking the following explicit approximations of the Schwarz primitive (P), Schwarz diamond (D), and Schoen gyroid (G) [5,47] on the unit domain:

$$\phi(x, y, z, 0) = 0.25\,(\cos(2\pi x) + \cos(2\pi y) + \cos(2\pi z))\,,$$

$$\begin{aligned}\phi(x, y, z, 0) &= 0.25\,(\cos(2\pi x)\cos(2\pi y)\cos(2\pi z)\\ &\quad - \sin(2\pi x)\sin(2\pi y)\sin(2\pi z))\,,\end{aligned}$$

$$\begin{aligned}\phi(x, y, z, 0) &= 0.25\,(\sin(2\pi x)\cos(2\pi y)\\ &\quad + \sin(2\pi z)\cos(2\pi x) + \sin(2\pi y)\cos(2\pi z))\,.\end{aligned}$$

It should be pointed out that the above explicit forms are neither minimal nor constant mean curvature surfaces [5]. For each case, we perform three tests of which the first two are performed with our proposed fourth-order scheme. In these two tests, the values of $\epsilon = 0.01$ and $\Delta t = 0.1h$ are chosen to be the same, but different spatial step sizes, namely $h = 1/64$ and $h = 1/128$ are used. In the third test, we use second-order schemes such as those introduced in [5] and choose the following parameters: $\epsilon = 0.01$, $h = 1/128$, and $\Delta t = h^2$.

Fig. 8(a)–(c) shows the Schwarz Primitive, Schwarz Diamond and Schwarz Gyroid at time $t = 0.1563$, respectively. Fig. 8(b) shows the zero contours of $\phi(x, 0.5, z)$ and Fig. 8(c) is the closed view of Fig. 8(b). These results suggest that our proposed method can generate a family of the triply periodic constant mean curvature surfaces. Furthermore, we find that the agreement between the solutions computed by second-order schemes with $h = 1/128$ and our proposed method with $h = 1/64$ is good. We also list the CPU time for the three cases in Table 2. These results indicate that the accuracy of the numerical solutions can be improved by using smaller time steps in the second-order scheme. Therefore, this approach required much more computational time than a fourth-order scheme.

3.8. Volume reconstruction from slice

We extend our proposed method to volume reconstruction from slice. Three-dimensional volume reconstruction from a sequence of medical images has numerous applications such as medical diagnostics, plastic and artificial limb surgery, and treatment

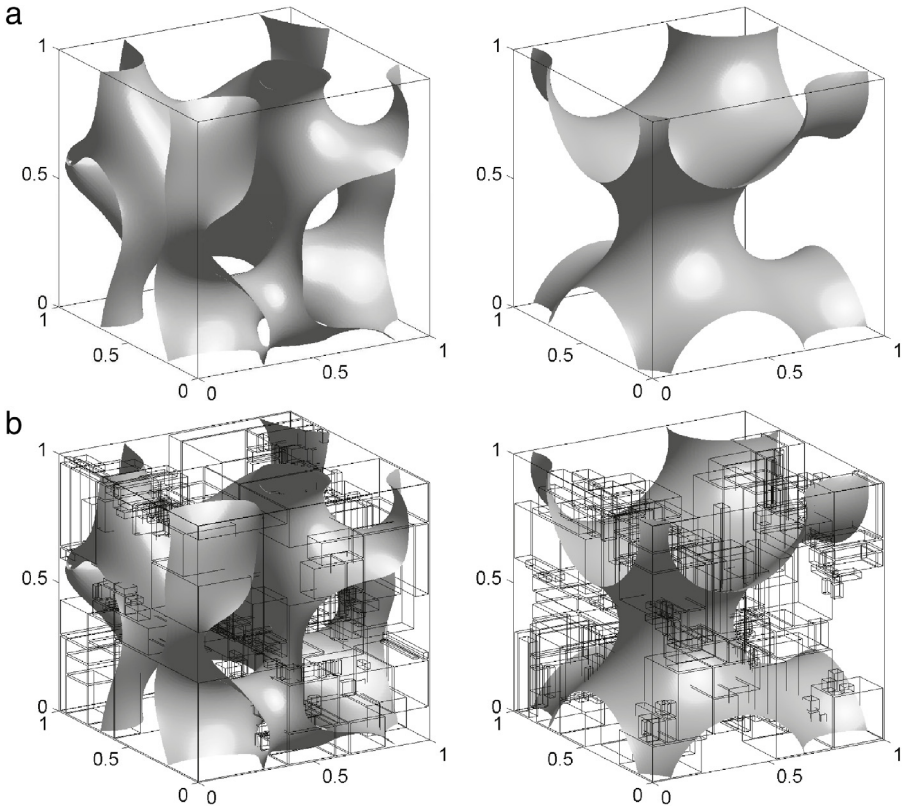

Fig. 7. Snapshots showing the adaptive mesh from the three-dimensional evolution. The zero-level grid has $16 \times 16 \times 16$ points and four levels of mesh refinement are used in the unit domain. (a) Zero isosurface of ϕ at time 1.26 and 10.08 from left to right. (b) Zero isosurface of ϕ with the adaptive mesh.

Table 2
Comparisons of CPU time using a second-order scheme [5] and our proposed fourth-order scheme.

Cases	Second-order scheme	Fourth-order scheme	Fourth-order scheme
Mesh size	$h = 1/128$	$h = 1/64$	$h = 1/128$
Time step	$\Delta t = h^2$	$\Delta t = 0.1h$	$\Delta t = 0.1h$
P surface	101 min	4 min	59 min
D surface	132 min	6 min	90 min
G surface	64 min	2 min	29 min

planning [48]. For three-dimensional volume reconstruction using slice data, we considered a modified Cahn–Hilliard equation containing a fidelity term [14]:

$$\frac{\partial \phi(\mathbf{x}, t)}{\partial t} = \Delta \mu(\mathbf{x}, t) + \lambda(\mathbf{x})(\psi(\mathbf{x}) - \phi(\mathbf{x}, t)), \tag{15}$$

$$\mu(\mathbf{x}, t) = F'(\phi(\mathbf{x}, t)) - \epsilon^2 \Delta \phi(\mathbf{x}, t), \tag{16}$$

where

$$\lambda(\mathbf{x}) = \begin{cases} \lambda_0, & \text{if } \mathbf{x} \text{ is in the given slice data,} \\ 0, & \text{otherwise.} \end{cases}$$

Here, $\phi(\mathbf{x}, t)$ is a phase-field function close to 1 or -1 for the respective interior and exterior of the reconstructed volume. The surface of the volume is represented by the zero-level set of ϕ. λ_0 is a positive value and $\psi(\mathbf{x})$ is the segmented image information from the input slice data obtained by using an image segmentation algorithm [49–51]. Further, $\lambda(\mathbf{x})(\psi - \phi)$ enforces ϕ to be the known data ψ in the input slice. The algorithms (15) and (16) have two features. One of which is that the values in the input slice are close to those in the original input slice. The second feature is that in the non-input slice, the values are obtained by curvature-driven diffusions and utilizing the volume information from the original (known) input slice data. Our proposed scheme can be extended to discretize Eqs. (15) and (16) as:

$$\begin{aligned} &\frac{1}{\Delta t}\left(\frac{3}{2}\phi^{n+1} - 2\phi^n + \frac{1}{2}\phi^{n-1}\right) = \Delta_c \mu^{n+1} \\ &\quad - \frac{h^2}{12\Delta t}\left(\frac{3}{2}\Delta_c \phi^{n+1} - 2\Delta_c \phi^n + \frac{1}{2}\Delta_c \phi^{n-1}\right) \\ &\quad + \frac{h^2}{12}\Delta_c(\lambda(\psi - \phi^n)), \end{aligned} \tag{17}$$

$$\begin{aligned} \mu^{n+1} &= 2(F'(\phi) - 2\phi)^n - (F'(\phi) - 2\phi)^{n-1} + 2\phi^{n+1} \\ &\quad - \epsilon^2 \Delta_c \phi^{n+1} + \frac{h^2}{12}\Delta_c \left(2(F'(\phi) - 2\phi)^n \right. \\ &\quad \left. - (F'(\phi) - 2\phi)^{n-1} + 2\phi^{n+1} - \mu^{n+1}\right). \end{aligned} \tag{18}$$

The size of slice image is 216×216 and we removed some similar slices (the empty boxes in Fig. 9(a)), see also [14]. There are seven slices between any two consecutive known slices. We perform the reconstruction on the domain $(0, 1) \times (0, 1) \times (0, 4.120)$ with a $216 \times 216 \times 890$ mesh grid. ϵ_4 and $\lambda_0 = 1000$ are chosen. Note that in this section, we use a homogeneous Neumann boundary condition to ensure that both the concentration and the

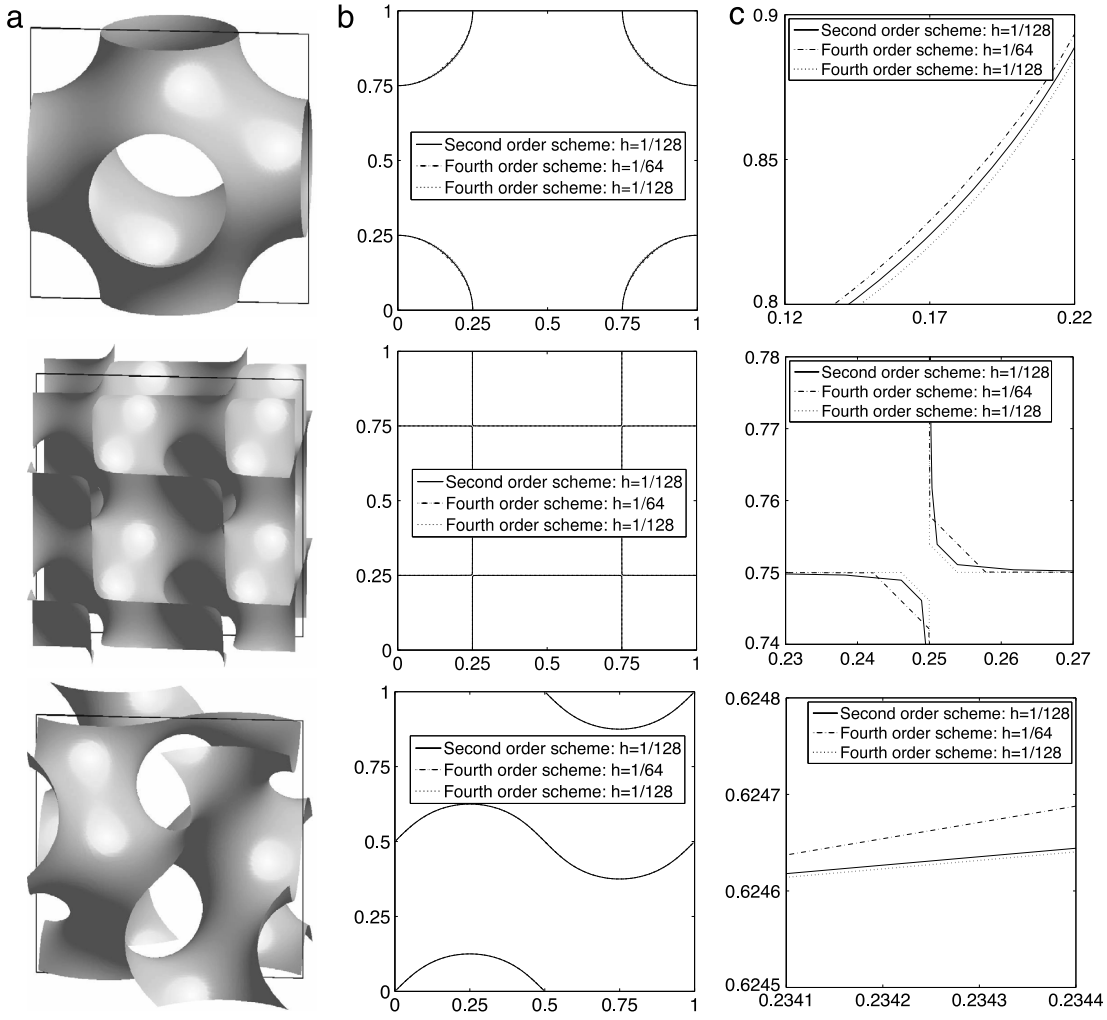

Fig. 8. Minimal surface of Schwarz Primitive, Schwarz diamond and Schwarz gyroid (from top to bottom) at time $t = 0.1563$. (a) Zero isosurfaces obtained by our proposed method with $h = 1/128$. (b) The zero contours of $\phi(x, 0.5, z)$. (c) Closed view of (b).

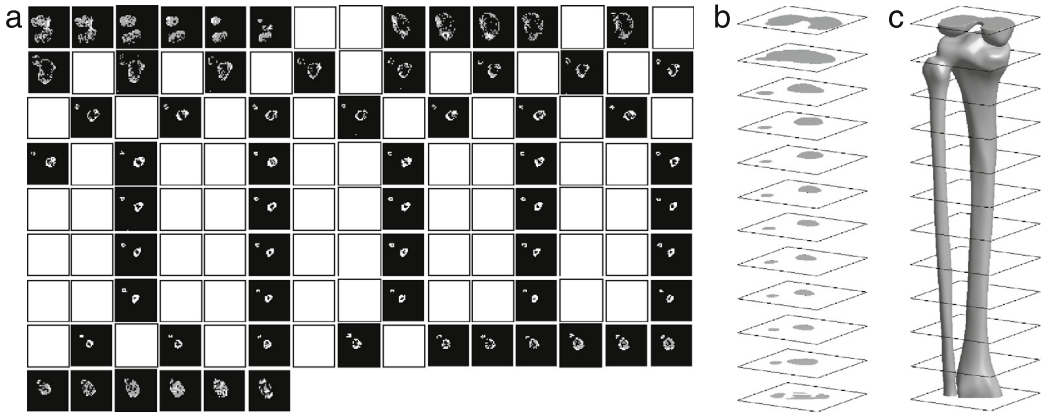

Fig. 9. Volume reconstruction from medical images of a human bone (tibia and fibula): (a) Slice data (ordered left to right and top to bottom), in which empty boxes represent skipped data, see also [14]. (b) Segmented images. Note that for improved visualization purposes, few segmented images from the slice data are displayed. (c) Reconstructed volume.

chemical potential corresponding to match the requirement of the volume reconstruction from slice. Fig. 9(c) shows the result of volume reconstruction from medical images of a human bone (tibia and fibula). As can be seen, our algorithm renders a good representation of the bone image and produces good visual quality.

4. Conclusions

In this paper, we extended the previous two-dimensional compact scheme for the Cahn–Hilliard equation to the three-dimensional space. The proposed scheme, derived by combining

a compact formula and linearly stabilized splitting scheme, has second-order accurate in time and fourth-order accurate in space. The discrete system can preserve the total mass and can use large time step sizes and exhibits excellent stability. In addition, our approach also provides a framework that can be extended to discretize most existing modified Cahn–Hilliard equations and adaptive mesh refinement framework. Several numerical experiments were performed to demonstrate the performance of the proposed algorithm.

Acknowledgments

Y.B. Li is supported by the Fundamental Research Funds for the Central Universities, China (No. XJJ2015068) and supported by China Postdoctoral Science Foundation (No. 2015M572541). The corresponding author (J.S. Kim) was supported by the National Research Foundation of Korea (NRF) grant funded by the Korea government (MSIP) (NRF-2014R1A2A2A01003683).

References

[1] J.W. Cahn, J.E. Hilliard, J. Chem. Phys. 28 (1958) 258–267.
[2] J.W. Cahn, J. Chem. Phys. 30 (1959) 1121–1124.
[3] A.J. Archer, R. Evans, J. Chem. Phys. 121 (9) (2004) 4246–4254.
[4] U.M.B. Marconi, P. Tarazona, J. Chem. Phys. 110 (16) (1999) 8032–8044.
[5] S.-D. Yang, H.G. Lee, J.K. Kim, Comput. Phys. Comm. 181 (2010) 1037–1046.
[6] V.E. Badalassi, H.D. Ceniceros, S. Banerjee, J. Comput. Phys. 190 (2003) 371–397.
[7] J. Kim, Commun. Comput. Phys. 12 (2012) 613–661.
[8] Z. Guo, P. Lina, Y. Wang, Comput. Phys. Comm. 185 (2014) 63–78.
[9] D. Han, X. Wang, J. Comput. Phys. 290 (2015) 139–156.
[10] N.J. Armstrong, K.J. Painter, J.A. Sherratt, J. Theoret. Biol. 243 (1) (2006) 98–113.
[11] S. Wise, J. Lowengrub, H. Frieboes, V. Cristini, J. Theoret. Biol. 253 (2008) 524–543.
[12] A.L. Bertozzi, S. Esedoglu, A. Gillette, IEEE Trans. Image Process. 16 (2007) 285–291.
[13] A.L. Bertozzi, S. Esedoglu, A. Gillette, Multiscale Model. Simul. 3 (2007) 913–936.
[14] Y. Li, J. Shin, Y. Choi, J. Kim, Comput. Vis. Image Underst. 137 (2015) 115–124.
[15] L.Q. Chen, Ann. Rev. Mater. Res. 32 (2002) 113–140.
[16] S. Dai, Q. Du, SIAM J. Appl. Math. 72 (2012) 1818–1841.
[17] D. Furihata, Numer. Math. 87 (2001) 675–699.
[18] Y. He, Y. Liu, T. Tang, Appl. Numer. Math. 57 (2007) 616–628.
[19] H. Gmez, V.M. Calo, Y. Bazilevs, T.J.R. Hughes, Comput. Method Appl. Math. 197 (2008) 4333–4352.
[20] H. Gomez, T.J.R. Hughes, J. Comput. Phys. 230 (2011) 5310–5327.
[21] D. Kay, R. Welford, J. Comput. Phys. 212 (2006) 288–304.
[22] H.G. Lee, J. Kim, Physica A 387 (2008) 4787–4799.
[23] Y. Li, D. Jeong, J. Shin, J. Kim, Comput. Math. Appl. 65 (2013) 102–115.
[24] S. Zhang, M. Wang, J. Comput. Phys. 229 (2010) 7361–7372.
[25] J.W. Stephenson, J. Comput. Phys. 55 (1984) 65–80.
[26] I. Altas, J. Dym, M.M. Gupta, R. Manohar, SIAM J. Sci. Comput. 19 (1998) 1575–1585.
[27] A.C. Radhakrishna Pillai, Internat. J. Numer. Methods Fluids 37 (2001) 87–106.
[28] Z.F. Tian, S.Q. Dai, J. Comput. Phys. 220 (2007) 952–974.
[29] J. Zhang, J. Comput. Phys. 179 (2002) 170–179.
[30] S. Zhai, X. Feng, Y. He, J. Sci. Comput. 54 (2013) 97–120.
[31] G. Sutmann, B. Steffen, J. Comput. Appl. Math. 187 (2006) 142–170.
[32] M. Li, T. Tang, J. Sci. Comput. 16 (2001) 29–45.
[33] E. Turkel, D. Gordon, R. Gordon, S. Tsynkov, J. Comput. Phys. 232 (2013) 272–287.
[34] J. Li, Z. Sun, X. Zhao, Sci. China Math. 55 (2012) 805–826.
[35] H. Song, Int. J. Comput. Math. 92 (2014) 2091–2108.
[36] C. Lee, D. Jeong, J. Shin, Y. Li, J. Kim, Physica A 409 (2014) 17–28.
[37] W.F. Spotz, G.F. Carey, Numer. Methods Partial Differential Equations 12 (1996) 235–243.
[38] U.M. Ascher, S.J. Ruuth, B.T.R. Wetton, SIAM J. Numer. Anal. 32 (1995) 797–823.
[39] D.J. Eyre, An unconditionally stable one-step scheme for gradient systems, Preprint. Available from: http://www.math.utah.edu/~eyre/research/methods/stable.ps.
[40] J. Kim, K. Kang, J. Lowengrub, J. Comput. Phys. 193 (2004) 511–543.
[41] C.M. Elliott, in: J.F. Rodrigues (Ed.), Mathematical Models for Phase Change Problems, in: International Series of Numerical Mathematics, vol. 88, Birkhauser-Verlag, Basel, 1989, pp. 35–73.
[42] A.S. Almgren, J.B. Bell, P. Colella, L.H. Howell, M.L. Welcome, J. Comput. Phys. 142 (1998) 1–46.
[43] M. Sussman, A.S. Almgren, J.B. Bell, P. Colella, L.H. Howell, M.L. Welcome, J. Comput. Phys. 148 (1999) 81–124.
[44] D.F. Martin, P. Colella, M. Anghel, F.L. Alexander, Comput. Sci. Eng. 7 (2005) 24–31.
[45] Y. Li, J. Kim, Int. J. Heat Mass Transfer 55 (2012) 7926–7932.
[46] Y. Li, D. Jeong, J. Kim, Meccanica 49 (2014) 239–252.
[47] P.J.F. Gandy, S. Bardhan, A.L. Mackay, J. Klinowski, Chem. Phys. Lett. 336 (2001) 187–195.
[48] J. Dornheim, D.J. Lehmann, L. Dornheim, B. Preim, G. Strauß, Reconstruction of Blood Vessels from Neck CT Datasets Using Stable 3D Mass–Spring Models, Eurographics Workshop on Visual Computing for Biology and Medicine, EG VCBM, 2008, pp. 77–82.
[49] T.F. Chan, L.A. Vese, IEEE Trans. Image Process. 10 (2) (2001) 266–277.
[50] Y. Li, J. Kim, Comput. Math. Appl. 62 (2) (2011) 737–745.
[51] Y. Li, J. Kim, Appl. Math. Comput. 219 (6) (2012) 3083–3090.